PERGAMON

International Journal of Heat and Mass Transfer 42 (1999) 2683–2694

International Journal of HEAT and MASS TRANSFER

Experimental and theoretical study of one- and two-component droplet vaporization in a high pressure environment

J. Stengele, K. Prommersberger*, M. Willmann, S. Wittig

Lehrstuhl und Institut für Thermische Strömungsmaschinen, Universität Karlsruhe (T.H.), Kaiserstraße 12, Postfach 6980, 76128 Karlsruhe, Germany

Received 17 June 1997; in final form 19 June 1998

Abstract

A new experimental set-up is introduced where the evaporation of free falling, non-interacting droplets is investigated. Detailed measurements with one- and two-component droplets are presented for different pressures ($p \to 40$ bar) and gas temperatures ($T \to 650$ K). The experimental results are compared with numerical calculations based on the Conduction Limit model and the Diffusion Limit model.

Nomenclature

B_m mass transfer number
B_T heat transfer number
c_p specific heat at constant pressure
c_w drag coefficient
d_d droplet diameter
D_g binary gaseous diffusivity
$D_{A,B}$ binary liquid diffusivity
F correction factor for relative change of film thickness
g gravity constant
L enthalpy of evaporation
Le Lewis number
m mass flow
n number of fuel components
Nu Nusselt number
p pressure
Pr Prandtl number
Q heat flux
r radial coordinate
r_d droplet radius
Re Reynolds number
t time
Sc Schmidt number
Sh Sherwood number
T temperature
u velocity
x distance
Y mass fraction.

Greek symbols

ε evaporation rate
λ thermal conductivity
ρ density
ω dimensionless radial coordinate.

Subscripts

crit critical
d droplet
f fuel vapour
g gas phase
i fuel component
ref reference
rel relative
s droplet surface
vap vaporisation
∞ infinity
0 initial state
0 without evaporating mass flow
* evaporating mass flow included.

* Corresponding author. Tel.: 0049 721 608 3242; fax: 0049 721 608 2767.

E-mail address: klans.prommersberger@its.uni-karlsruhe.de (K. Prommersberger)

0017–9310/99/$ - see front matter
PII: S0017–9310(98)00285–3

1. Introduction

The combustion of liquid fuels in thermal engines is mainly influenced by the atomization of the liquid fuel, the motion and evaporation of the fuel droplets, and the mixing of fuel and air. Since the pressure level of the combustion engine has to be elevated to increase thermal efficiency, these processes take place typically in a high pressure environment. In modern gas turbine engines, for example, the pressure inside the combustion chamber reaches or even exceeds the critical pressure of the fuel used. In the past many experimental studies have been done in order to characterise the behaviour of evaporating fuel sprays [1–4]. They all found that spray modelling strongly depends on correct prediction of the droplet motion and evaporation.

Typical fuels consist of many different hydrocarbons and it is shown in Law et al. [5] and Sirignano and Law [6], that the evaporation process of the fuel mixture cannot be described correctly by one-component fuels. This is due to the great variety of the thermophysical and chemical properties and the different volatilities of the fuel components. Especially during cold starting conditions of the engine, when the temperature of the ambient gas is low, the highly volatile components of the fuel play an important role for ignition and burning processes of the engine.

Numerous theoretical studies have been carried out describing droplet evaporation in a high pressure gas [7–11]. They take into account the real gas behaviour, the variation of the thermophysical properties, the non-ideality of the latent heat of evaporation and the non-ideal phase equilibrium including the solubility of the ambient gas inside the droplet. These points are found to be extremely important for the correct prediction of the droplet evaporation in high pressure environments. Since the droplet temperature rises with increasing pressures, the unsteady heating of the droplet affects significantly the droplet evaporation process under high pressure conditions and steady state evaporation cannot be obtained. If the pressure and the temperature of the gaseous environment is sufficiently high, the droplet may reach the critical point during its evaporation time. These conditions are reached for example in liquid oxygen combustion systems. Delplanque and Sirignano [13] apply new evaporation models in this region, since the surface tension and the heat of evaporation become zero. However, Hsieh et al. [8] found in a theoretical study that for pentane droplets subcritical models can be used up to 65 bar.

Only a few experimental studies have been published describing the droplet evaporation process in high pressure environments [14–16]. In order to exclude gravity and convective effects on the evaporation process some experiments on high pressure droplet vaporisation were carried out in microgravity environments. These experiments have been conducted with droplets attached to a thin fiber resulting in the impairment of the droplet evaporation process due to the suspension unit. Shih and Megaridis [19] have shown that these kinds of experiments will lead to an overestimation of the liquid evaporation rates and underprediction of the droplet lifetimes.

No experiments considering two- or multi-component droplet evaporation in high pressure atmosphere have been published yet. The present study is intended to describe the evaporation of one- and two-component droplets in a high pressure environment by experimental methods and numerical simulation. Two-component droplets are chosen as a simplification to describe the influence of the liquid mixture and the different volatilities of the components on the evaporation process.

The present study introduces a new experimental set-up where the evaporation of free falling droplets in a stagnant high pressure gas is investigated. There is no need of a suspension of the droplet and the evaporation process can be observed without any disturbing influence. Since the distance between the evaporating droplets is large, there is no interaction of the droplets. Due to the relative velocity between the falling droplet and the stagnant gas, convective effects have to be taken into consideration by experimental correlations. The experimental conditions of droplet size, droplet initial temperature, ambient temperature and pressure were chosen to achieve a significant effect of multicomponent fuels on the evaporation process. In comparison with a combustor spray, the free falling droplets are one order of magnitude larger but their velocities are lower. Therefore the Reynolds number is comparable to conditions of combustion chambers.

In order to describe the convective effects, the theory of Abramzon and Sirignano [20] is combined with the experimental correlation of Ranz and Marshall [21]. The experimental results are compared with the Conduction Limit model of Law and Sirignano [22] and the Diffusion Limit model of Landis and Mills [23] assuming only diffusive heat and mass transport within the droplet. Aggarwal [24], Tong and Sirignano [25] and Jin and Borman [26] showed theoretically, that the influence of a flow inside the droplet on transport processes is of minor importance compared to the internal radial diffusional heat and mass transport. This is also confirmed by the experimental study of Stengele et al. [27] for heptane droplets.

2. Droplet evaporation model

The present model describes the evaporation process of an isolated evaporating droplet in a convective flow field. The flow around the droplet is assumed to be laminar. Variable thermophysical properties have been used inside the droplet and the surrounding gas to account for

Table 1
Thermophysical properties of gases and liquids [29, 30]

Property	Method	Pressure correction	Mixing rule
Liquid properties			
Density	Hankinson and Thomson	Thomson et al.	Hankinson and Thomson
Specific heat capacity	Rowlinson	—	Teja
Dynamic viscosity	Van Velzen et al., Letsou and Stiel	Lucas	Grunberg and Nissan
Thermal conductivity	Jamieson	Lenoir	Li
Diffusion coefficient	Vignes, Hayduk and Minhas	—	Perkins and Geankoplis
Gas phase properties			
Density	Soave–Redlich–Kwong	Soave–Redlich–Kwong	van der Waals mixing rule
Specific heat capacity	Polynom 3. degree	Lee and Kesler	Plocker et al.
Dynamic viscosity	Lucas	Lucas	Lucas
Thermal conductivity	Roy and Thodos, Miller et al.	Stiel and Thodos	Yorizane et al.
Diffusion coefficient	Fuller et al.	Takahashi	Bird et al.

the variation of temperature and concentration [28]. The correlations necessary to determine the physical properties are taken from Reid et al. [29, 30] and listed in Table 1. The following simplifications are assumed in the model: the droplet evaporates in an inert atmosphere. The interface between liquid and gas phase is assumed to be in thermodynamic equilibrium. Radiative heat transfer is neglected [31]. Fick's law is used to calculate mass diffusion. Dufour and Soret effects are not considered. The evaporation process is assumed to be spherically symmetric, the asymmetric convective effects on the evaporation process are included implicitly in the correlations of Ranz and Marshall [21].

2.1. Gas phase equations

In the present model the gas phase is assumed to be quasi-steady. Delplanque [32] showed that this assumption is valid for typical high pressure spray application, since the characteristic time of the flow around the droplet is much smaller than the droplet lifetime. Applying the integral solution of the governing equations [33] and the extended film theory of Abramzon and Sirignano [20] the evaporating mass flow of the droplet and the heat transfer from the hot environment towards the droplet are calculated as follows.

The convective effects on the heat and mass transfer of the evaporating droplet are determined by equations (1) and (2).

$$Nu^* = 2 + \frac{Nu_0 - 2}{F(B_T)} \tag{1}$$

$$Sh^* = 2 + \frac{Sh_0 - 2}{F(B_m)} \tag{2}$$

The radially outward directed flow of evaporating droplet is described by correction factors for heat transfer $F(B_m)$ and mass transfer $F(B_T)$.

$$F(B_m) = (1 + B_m)^{0.7} \frac{\ln(1 + B_m)}{B_m} \tag{3a}$$

$$F(B_T) = (1 + B_T)^{0.7} \frac{\ln(1 + B_T)}{B_T} \tag{3b}$$

The correlations of Ranz and Marshall [21] are used to calculate Nu_0 and Sh_0 in equations (1) and (2).

$$Nu_0 = 2 + 0.6\sqrt{Re_d}\, Pr^{1/3} \tag{4}$$

$$Sh_0 = 2 + 0.6\sqrt{Re_d}\, Sc^{1/3} \tag{5}$$

The evaporating mass flow of the droplet is obtained by the integrations of the quasi-steady energy and mass equations.

$$\dot{m}_{vap} = 2\pi r_d \frac{\lambda_{g.ref}}{c_{p_{g.ref}}} Nu^* \ln(1 + B_T) \tag{6}$$

$$\dot{m}_{vap} = 2\pi r_d \rho_{g.ref} D_{g.ref} Sh^* \ln(1 + B_m) \tag{7}$$

where B_T and B_m are the Spalding heat and mass transfer numbers.

$$B_T = \frac{\dot{m}_{vap} c_{p_{g.ref}} (T_{g,\infty} - T_{g,s})}{Q_{tot}} \tag{8}$$

The mass flow rate of the fuel vapour components and the mass transfer number is determined by equations (9) and (10).

$$1 + B_m = \frac{\sum_{i=1}^{n} Y_{i,f,\infty} - 1}{\sum_{i=1}^{n} Y_{i,f,s} - 1} = \frac{Y_{i,f,\infty} - \varepsilon_i}{Y_{i,f,s} - \varepsilon_i} \tag{9}$$

$$\varepsilon_i = \frac{\dot{m}_{\mathrm{vap},i}}{\dot{m}_{\mathrm{vap}}}, \quad \sum_i^n \varepsilon_i = 1 \tag{10}$$

In contrast to the theory of Abramzon and Sirignano [20], the specific heat capacity of the pure vapour is replaced by the specific heat capacity of the vapour/gas mixture. The thermophysical properties necessary are obtained by the 1/2-rule of Renksizbulut and Yuen [34]. The only exception is the gas density of the Reynolds number, which is calculated at free stream conditions [35]. Combining equations (6) and (7) the following relationship is obtained.

$$B_{\mathrm{T}} = (1+B_{\mathrm{m}})^{1\,Sh^*/Le_{\mathrm{g}}Nu^*} - 1 \tag{11}$$

The calculation procedure starts from equation (7) where the evaporating mass flow of the liquid fuel is calculated. From this, B_{T} is determined by equation (11). This has to be done by iteration. Then, the total heat transfer from the surrounding gas towards the droplet is calculated using equation (8).

2.2. Droplet motion

The equation of droplet motion is obtained by the balance of forces. For reasons of simplicity, the motion of the droplet and the gas flow is assumed to be one-dimensional. The gravity forces and the buoyancy forces are also included, since they affect the evaporation process of the droplet in the experiments presented here.

$$\frac{\mathrm{d}u_{\mathrm{d}}}{\mathrm{d}t} = -\frac{3}{4}\frac{\rho_{\mathrm{g}}}{\rho_{\mathrm{d}}}\frac{c_{\mathrm{w}}}{d_{\mathrm{d}}}u_{\mathrm{rel}}(u_{\mathrm{d}}-u_{\mathrm{g}}) + \left(1-\frac{\rho_{\mathrm{g}}}{\rho_{\mathrm{d}}}\right)g \tag{12}$$

The drag coefficient is calculated by the correlation of Renksizbulut and Haywood [36] where the flow of the evaporating fuel radially outward is included. The Reynolds number is calculated again with the free stream density [35].

$$c_{\mathrm{w}}(1+B_{\mathrm{m}})^{0.2} = 0.36 + 5.48 \cdot Re_{\mathrm{d}}^{-0.573} + \frac{24}{Re_{\mathrm{d}}} \tag{13}$$

After solving equation (12) the position of the evaporating droplet is determined from kinematics.

$$\frac{\mathrm{d}x_{\mathrm{d}}}{\mathrm{d}t} = u_{\mathrm{d}} \tag{14}$$

2.3. Liquid phase equations

In the present paper the Conduction Limit model [22] and the Diffusion Limit model [23] are used to describe the heat transport inside the droplet. Since convection within the droplet is neglected, the liquid phase equations reduce to the conservation of species and energy. For one-component droplets (Conduction Limit model) only the conservation of energy has to be considered. The describing differential equations have to be solved numerically.

$$\rho_{\mathrm{d}}c_{\mathrm{p,d}}\frac{\partial T_{\mathrm{d}}}{\partial t} = \frac{1}{r^2}\frac{\partial}{\partial r}\left(r_{\mathrm{d}}^2\lambda_{\mathrm{d}}\frac{\partial T_{\mathrm{d}}}{\partial r}\right) \tag{15}$$

$$\frac{\partial(Y_{i,\mathrm{d}}\rho_{\mathrm{d}})}{\partial t} = \frac{1}{r^2}\frac{\partial}{\partial r}\left(\rho_{\mathrm{d}}r^2 D_{\mathrm{A,B}}\frac{\partial Y_{i,\mathrm{d}}}{\partial r}\right) \tag{16}$$

The instantaneous droplet diameter is derived from the mass balance around the droplet.

$$\frac{\mathrm{d}r_{\mathrm{d}}}{\mathrm{d}t} = -\frac{1}{\rho_{\mathrm{d,s}}r_{\mathrm{d}}^2}\left(\frac{\dot{m}_{\mathrm{vap}}}{4\pi} + \int_0^{r_{\mathrm{d}}}\frac{\partial\rho_{\mathrm{d}}}{t}r^2\,\mathrm{d}r\right) \tag{17}$$

Since the droplet diameter changes during the evaporation process, the radial coordinate in the gas phase and liquid phase is non-dimensionalized by the instantaneous droplet diameter. With this transformation the droplet surface is always located at $\omega = 1$ resulting in the simpler solution procedures of equations (15) and (16).

$$\omega = \frac{r}{r_{\mathrm{d}}(t)} \tag{18}$$

In order to determine the temperature and fuel distribution inside the droplet the following initial and boundary conditions are applied. The initial temperature and concentration within the droplet is assumed to be uniform. The boundary conditions result from symmetry at the droplet centre and the conservation of energy and mass at the droplet surface. These are expressed in terms of Neumann conditions.

$$\left.\frac{\partial T_{\mathrm{d}}}{\partial r}\right|_{r=0} = 0 \tag{19}$$

$$\left.\frac{\partial Y_{i,\mathrm{d}}}{\partial r}\right|_0 = 0 \tag{20}$$

$$\rho_{\mathrm{d}}D_{\mathrm{AB}}\left.\frac{\partial Y_{i,\mathrm{d}}}{\partial r}\right|_{\mathrm{s}} = \frac{1}{4\pi r_{\mathrm{d}}^2}(\dot{m}_{\mathrm{vap}}Y_{i,\mathrm{d,s}} - \dot{m}_{\mathrm{vap,i}}) \tag{21}$$

$$4\pi r_{\mathrm{d}}^2\lambda_{\mathrm{d}}\left.\frac{\partial T_{\mathrm{d}}}{\partial r}\right|_{r_{\mathrm{d}}} = \dot{Q}_{\mathrm{tot}} - \dot{m}_{\mathrm{vap}}L \tag{22}$$

where $\dot{Q}_{\mathrm{tot}}$ is the total heat flux in equation (9) and $\dot{m}_{\mathrm{vap}}L$ represents the latent heat of evaporation.

2.4. Phase equilibrium at high pressure

This model assumes that the gas/liquid interface is in thermodynamic equilibrium. In contrast to low pressure applications, where Raoul's law is valid, the determination of the phase equilibrium in high pressure environments has to consider real gas effects and the solubility of the ambient gas inside the droplet. Additionally, in high pressure applications the latent heat of evap-

oration is a function of pressure and temperature as well. These effects are described in a previous paper [11], in detail. In the present study the gas dissolved within the droplet is confined in the outermost layer of the droplet. It turned out that the gas diffusing towards the droplet centre does not affect the evaporation process of the droplet.

2.5. Solution procedure

An implicit scheme is used to discretise the differential equation within the droplet resulting in a linear equation, which is solved directly by a TDMA solution procedure (Tridiagonal Matrix Algorithm) [37]. A uniformly spaced grid with 100 grid points is applied. The accuracy of the calculated solution is strongly dependent on the magnitude of the chosen time step. It is limited to a maximum by three different criteria:

- The increase of the droplet temperature during one time step is limited to a maximum. This is important at the beginning of the evaporation process, when the droplet heats up rapidly.
- The maximum diameter regression may not be exceeded. This criterion is applied towards the end of the evaporation process, when the diameter regression of the droplet is high.
- The time step is generally limited to a maximum.

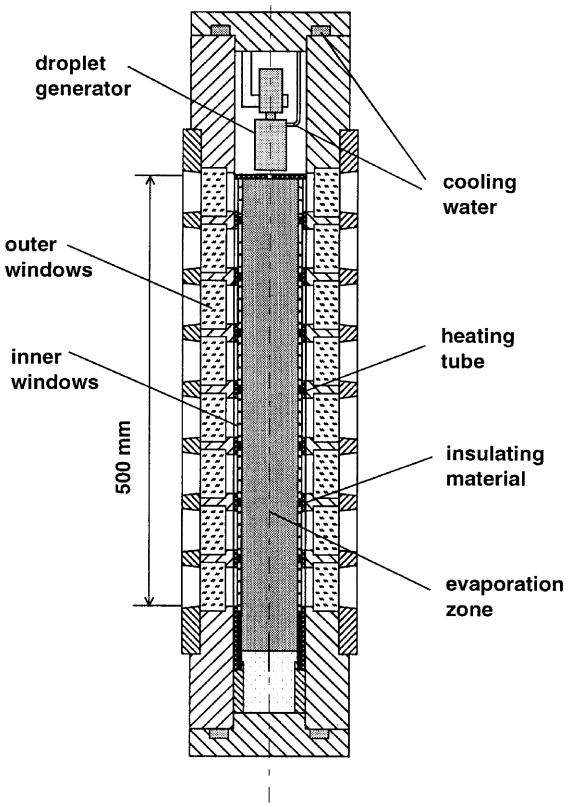

Fig. 1. Pressure chamber.

3. Experimental set-up

For the experimental verification of the droplet evaporation model a new test section was built where single droplets evaporate under well defined conditions. The maximum pressure inside the pressure chamber is 40 bar, the maximum temperature 700 K. Nitrogen is chosen as the test gas in order to exclude any combustion processes.

Figure 1 shows the cross-sectional view of the cylindrical pressure chamber. Within the pressure chamber a heating tube was inserted wherein the droplets evaporate. The heating tube is operated by two isolated electrical resistance wires with a power of 2200 W each. One wire heats the upper part of the evaporation zone, the other wire the lower part. In order to minimise heat losses and temperature gradients within the evaporation zone, insulating material has been put between the heater and the pressure chamber, and additional windows (inner windows) have been inserted in the heating tube.

The total length of the evaporation zone is 500 mm, the diameter is 65 mm. With these dimensions droplet/wall interactions are excluded. The evaporation of the droplets is observed through quartz glass windows. The instantaneous size and the velocity of the droplets are measured simultaneously by video technique and a stroboscope lamp. The diameter of the droplet is determined by a fixed enlargement factor of the optical set-up. The biggest lens aperture was chosen to minimise errors by the depth of focus. The velocity of the droplet is obtained by the known flash frequency of the stroboscope lamp and the distance between the two shadow images of the same droplet in one interlace picture. Since the droplets enter the evaporation zone with identical conditions, the measurements can be conducted at different positions in different times. The smallest droplet size detectable was approximately 300 μm. At this point over 90% of the initial droplet mass is evaporated. Measurements with smaller droplets turned out to be difficult, since minor inhomogenities in the gas phase affect the movement of the droplet and the evaporation distance significantly. The accuracy of the measuring systems was ± 20 μm for the droplet size and ± 0.05 m s^{-1} for the droplet velocity. The standard deviation of the measurements varied between 2 and 8%.

The droplets are generated in the upper part of the pressure chamber and fall down due to gravity through the high temperature stagnant nitrogen gas. In Fig. 2 the schematic view of the droplet generator is shown. Due to constant fuel mass flow through a thin glass capillary tube a droplet is generated at its tip. The diameter of the droplet increases until the weight of the droplet exceeds

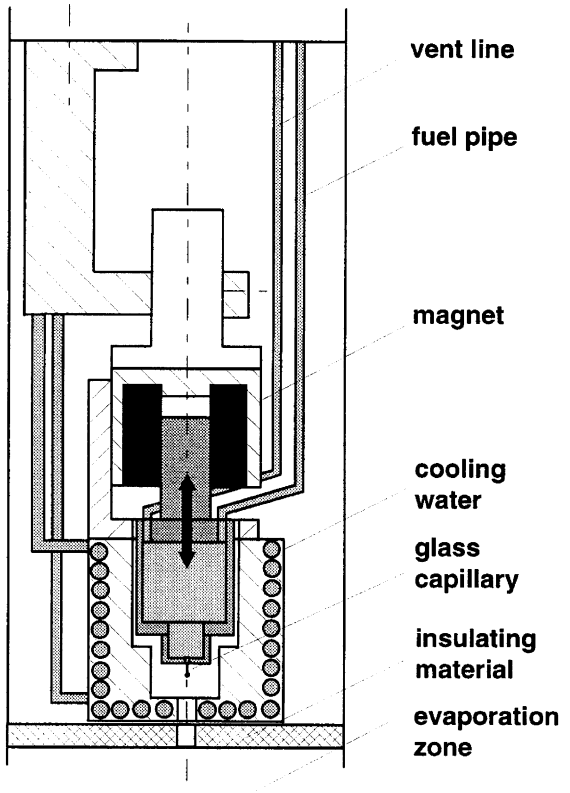

Fig. 2. Droplet generator.

the cohesion forces, the droplet separates from the capillary tube and enters the evaporation zone. With this static technique droplet diameter are limited to 1 mm or larger, since the diameter of the capillary can not be decreased.

With a forced separation the droplet size can be further reduced. This is realised by a movable droplet generator lifted by an electromagnet and then released again hitting a stroke device. The droplet falls off the glass capillary tube and enters the evaporation zone. With this technique droplets are produced in a diameter range between 600 and 900 μm. If the mass flow through the capillary tube is constant and the frequency of the up and down movement of the droplet generator is also constant, monodisperse droplets are produced. Constant differential pressure between the fuel tank and the pressure chamber is crucial to obtain constant mass flows. Depending on the frequency and the mass flow, the distance between the droplets can be adjusted arbitrarily within distinct boundaries. In the present study, the droplet distance was more than 100 times the initial droplet diameter, therefore, any interaction between the evaporating droplets was excluded. Inside the cavity surrounding the glass capillary, a thermocouple element is inserted close to the capillary tip to determine the initial temperature of the droplet. This temperature is important for the comparison of the numerical and experimental results. The droplet generator is cooled by water in order to keep constant the droplet initial temperature. To avoid blocking by trapped nitrogen, the droplet generator is vented regularly by means of a valve.

In Fig. 3 an overview of the whole test section is shown including all temperature and pressure measuring locations. In addition, valves, piping, heaters (H1 and H2) and control units are presented. In order to compensate pressure fluctuations a gas reservoir was connected to the fuel tank. The pressure difference between fuel tank and pressure chamber is measured permanently. Before filling with nitrogen gas, the test section is evacuated to avoid any residual oxygen inside the evaporation zone.

4. Results

The experiments with two-component droplets were carried out with binary mixtures of *n*-pentane and *n*-nonane. Two different initial droplet mixtures ($Y_{d,0,pentane} = 0.3$, $Y_{d,0,nonane} = 0.7$ and $Y_{d,0,pentane} = 0.7$, $Y_{d,0,nonane} = 0.3$) were investigated. For comparison and limiting cases, experiments with one-component droplets consisting of *n*-pentane or *n*-nonane were conducted. More results of one-component droplet evaporation can be found in [27]. The gas pressure of the nitrogen environment was $p = 20$, 30 and 40 bar, the gas temperature $T_\infty = 500$ K and 650 K. The initial droplet diameters varied between $d_{d,0} = 640$ and 820 μm.

For $p = 40$ bar and $T_\infty = 650$ K, the critical pressure and the critical temperature of the droplet components were exceeded ($T_{crit,pentane} = 470$ K, $p_{crit,pentane} = 33.7$ bar and $T_{crit,nonane} = 595$ K, $p_{crit,nonane} = 23.1$ bar). However, the calculated droplet temperature was well below the critical temperature of the fuel mixture.

In the following figures, the diameter and the velocity of the droplet are plotted over the evaporation distance. The symbols indicate the measured values, and the solid lines represent the calculated values. The initial droplet velocity results from the droplet acceleration between the glass capillary and the entrance of the evaporation zone. It is for all conditions approximately the same, $u_{d,0} = 0.5$ m s^{-1}. The initial droplet temperature rises slightly with higher pressures and higher gas temperatures. This effect occurs due to the intensified heat transfer from the evaporation zone towards the droplet generator.

4.1. Variation of gas pressure

A comparison of the experimental and theoretical results is shown in Fig. 4. In this case the initial droplet composition is $Y_{d,0,pentane} = 0.3$ and $Y_{d,0,nonane} = 0.7$ and the gas temperature is $T_\infty = 550$ K. The gas pressure varies between 20 and 40 bar, the initial droplet tem-

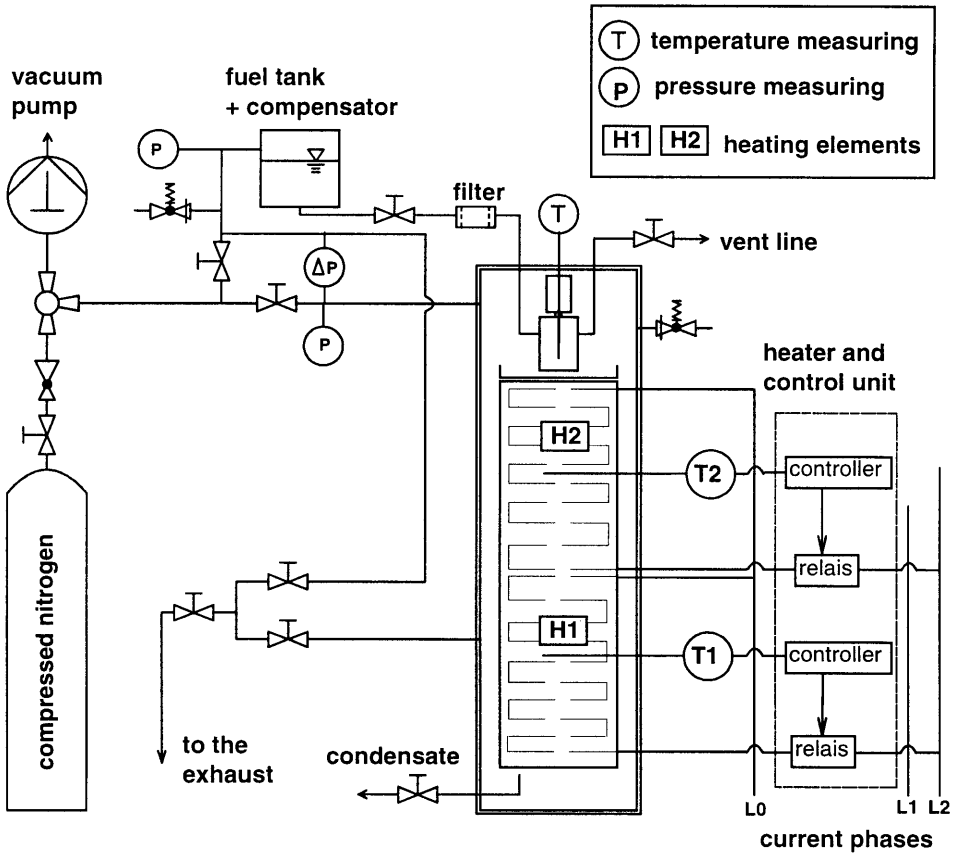

Fig. 3. Test section.

perature between $T_{d,0} = 370$ and 400 K, and the initial droplet diameter between $d_{d,0} = 650$ and 700 μm.

With elevating pressures the evaporation distance and the velocity of the droplet decreases. This results from the increased aerodynamic force at higher pressures. Similar velocity and diameter distributions are observed for all pressures. Due to the large droplet diameters at the beginning of the evaporation process, the droplet velocity increases quickly to its maximum. The magnitude depends on the gas pressure, the higher the gas pressure the lower the velocity maximum. Passing the point, the droplet velocity decreases since the aerodynamic resistance exceeds the force of gravity due to smaller droplet diameters. Towards the end of the evaporation process there is a steep velocity gradient. In this region the influence of gravity is negligible.

For all pressures investigated, there is an excellent agreement of the measured and calculated droplet diameter and velocity distributions.

4.2. *Variation of gas temperature*

The calculated and measured results also coincide very well for different gas temperatures (Fig. 5). Elevating the gas temperature, the evaporation distance of the droplet shortens. During the first part of the evaporation process the velocity increases with higher gas temperatures resulting from smaller aerodynamic resistance. However, the following reduction in droplet velocities is much steeper for higher temperatures due to the faster decrease of the droplet diameter.

In this case the initial droplet composition is $Y_{d,0,pentane} = 0.7$ and $Y_{d,0,nonane} = 0.3$ and the gas pressure is $p = 30$ bar. The gas temperature is $T_\infty = 550$ K and $T_\infty = 650$ K, the initial droplet temperature $T_{d,0} = 370$ K and $T_{d,0} = 380$ K, and the initial droplet diameter $d_{d,0} = 800$ and 820 μm.

4.3. *Variation of initial droplet diameter*

The decisive influence of the initial droplet diameter on the droplet evaporation process is shown in Fig. 6. Reducing the initial droplet diameter by 10% (from $d_{d,0} = 800$ to 720 μm) the evaporation distance shortens more than 25%. In this case the gas temperature is $T_\infty = 550$ K, the pressure $p = 30$ bar, the initial droplet temperature $T_{d,0} = 370$ K and the initial droplet com-

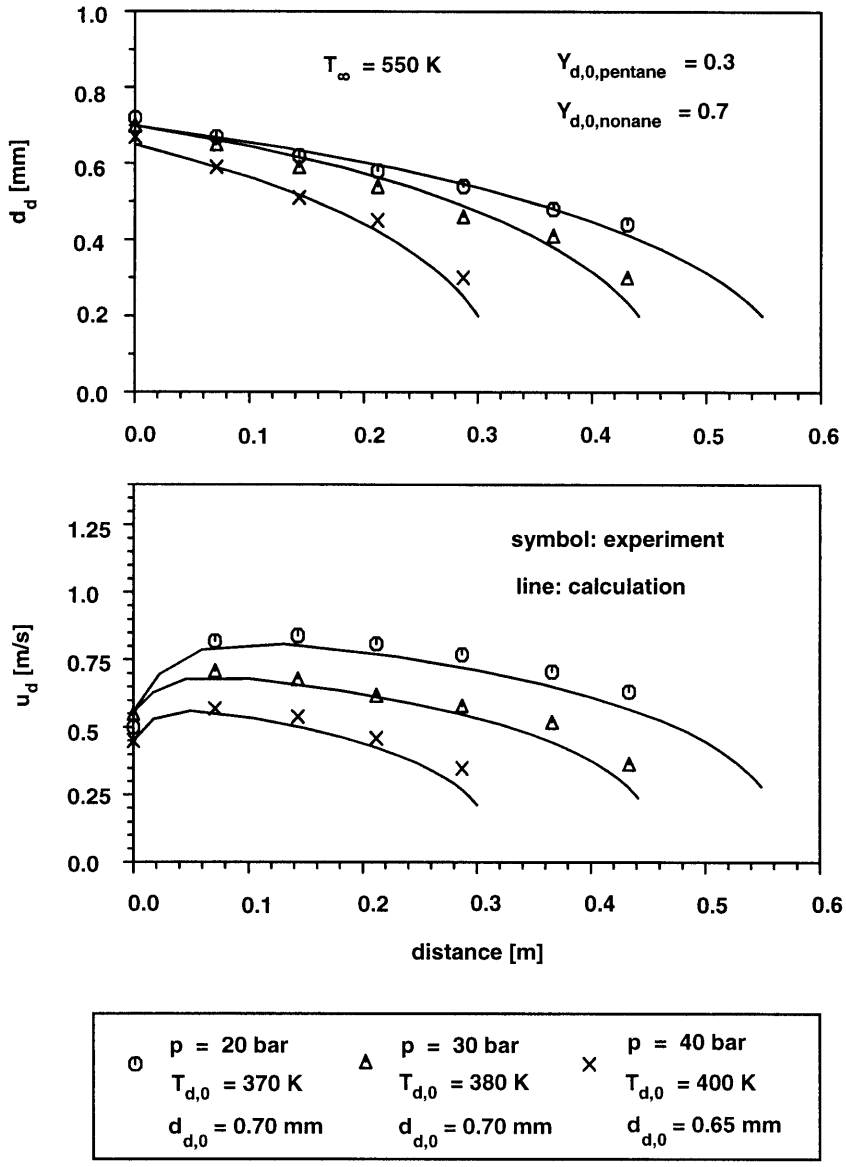

Fig. 4. Variation of gas pressure.

position is $Y_{d,0,pentane} = 0.7$ and $Y_{d,0,nonane} = 0.3$. As observed before, experiment and model agree very well.

4.4. Variation of fuel

In Fig. 7 the numerical and experimental results for one- and two-component droplets are shown. Different initial mixtures of two-component droplets consisting of $Y_{d,0,pentane} = 0.7$ and $Y_{d,0,nonane} = 0.3$ or $Y_{d,0,pentane} = 0.3$ and $Y_{d,0,nonane} = 0.7$ and the limiting cases of one-component droplets consisting of pentane or nonane are investigated to determine the influence of different fuel volatilities on the evaporation process of the droplet. From Fig. 7 it is obvious, that increasing the volatility of the fuel shortens the evaporation distance in the droplet.

In this case the gas temperature is $T_\infty = 550$ K, the gas pressure $p = 30$ bar, the initial droplet temperature $T_{d,0} = 380$ K. The initial droplet diameter varies between $d_{d,0} = 630$ and 740 μm. Again, experiment and theory agree very well (the velocity distribution is not shown explicitly).

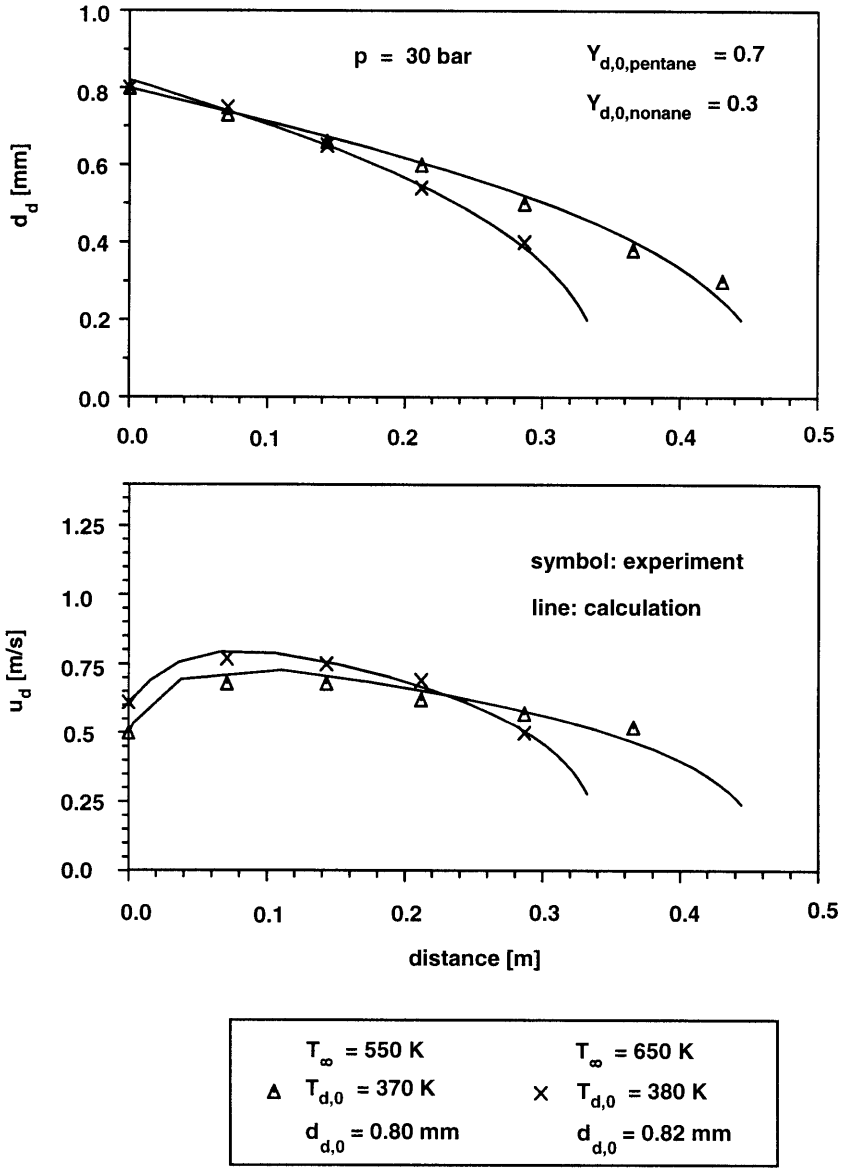

Fig. 5. Variation of gas temperature.

5. Conclusions

A new experimental set-up is presented where the evaporation of free falling, non interacting droplets is investigated. There is no need of a droplet suspension unit and the evaporation of the droplet can be observed without any disturbing influence. The new design of the droplet generator allows the production of monodisperse droplets in a size range of 600–900 μm initial diameter. Since the distance between the droplets is more than $100d_{d,0}$, interaction of the different droplets does not occur during the evaporation process.

Detailed measurements were conducted with one- and two-component droplets at different gas pressures ($p = 20$, 30 and 40 bar) and gas temperatures of 550 and 650 K. The initial droplet diameter was varied between 640 and 820 μm. The experiments were carried out with binary mixtures of *n*-pentane and *n*-nonane. Two different initial droplet mixtures ($Y_{d,0,pentane} = 0.3$, $Y_{d,0,nonane} = 0.7$ and $Y_{d,0,pentane} = 0.7$, $Y_{d,0,pentane} = 0.3$) were inves-

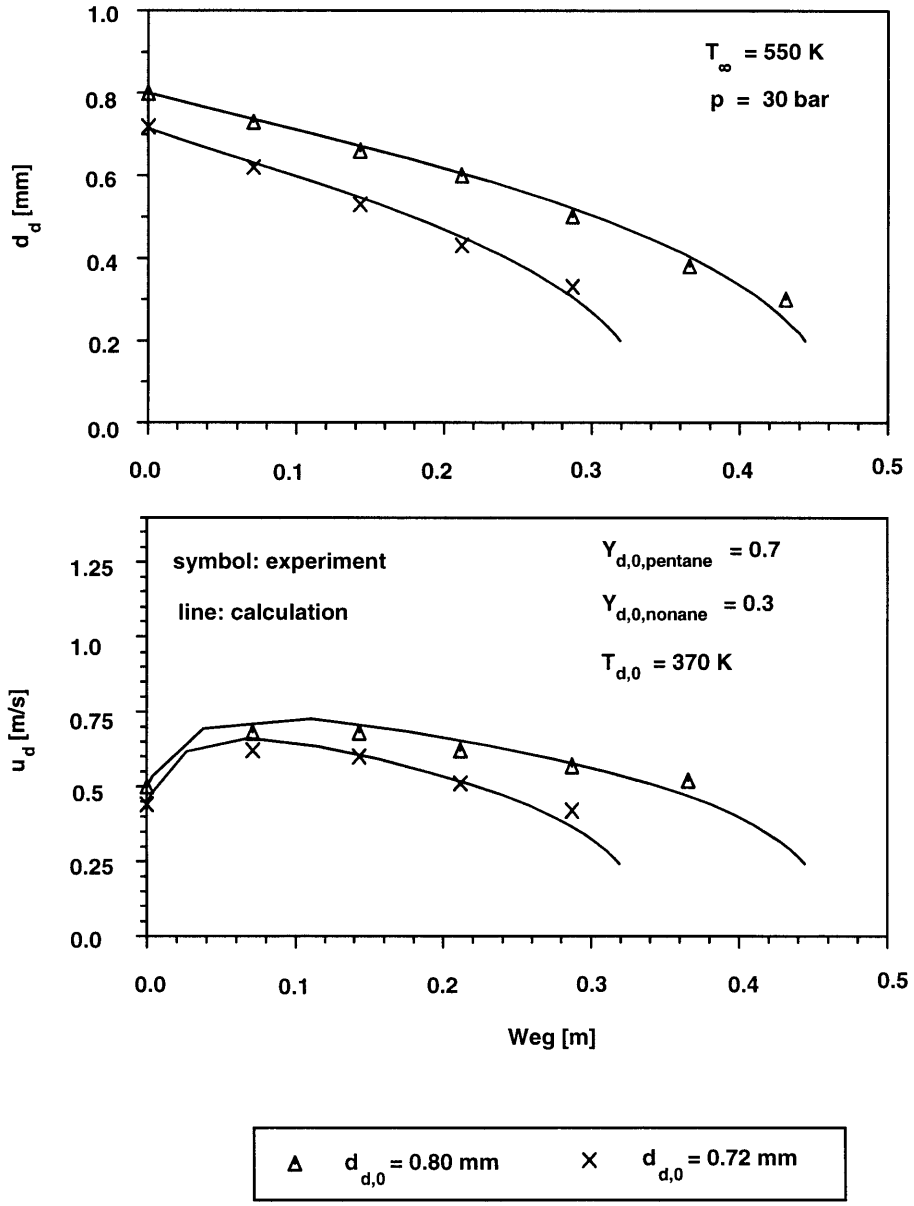

Fig. 6. Variation of initial droplet diameter.

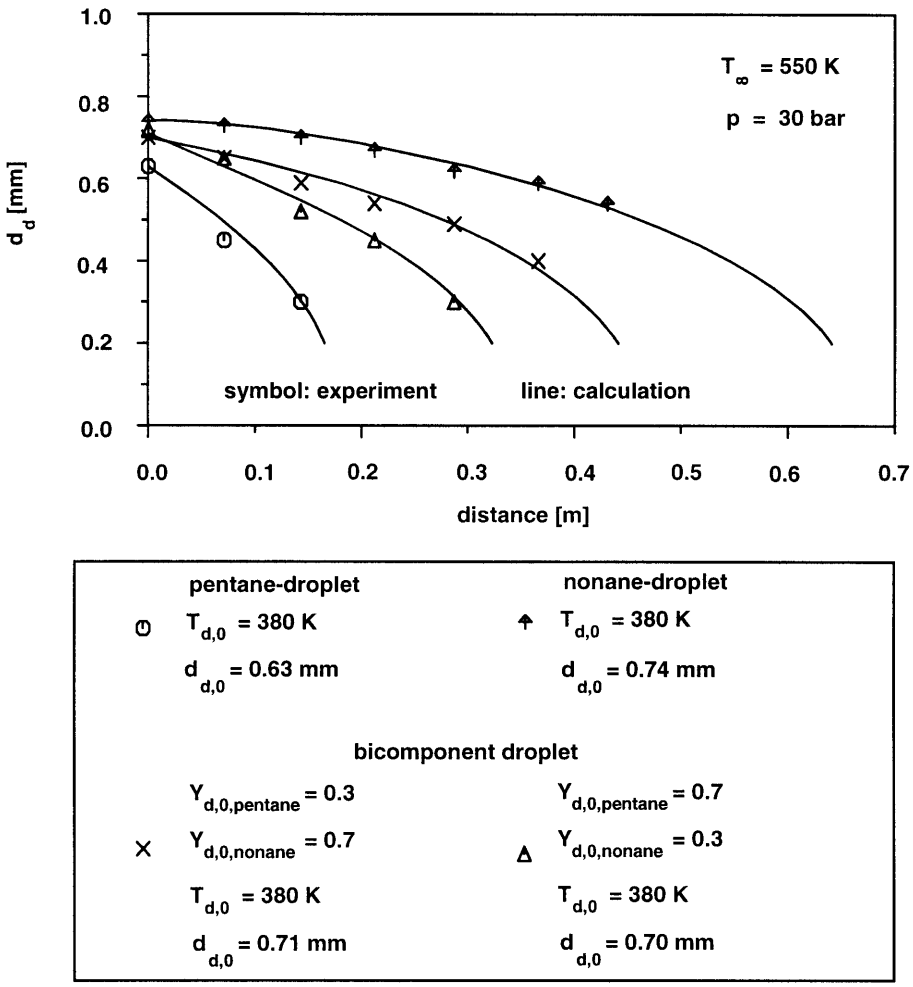

Fig. 7. Fuel variation.

tigated. Additionally, experiments with one-component droplets consisting of pure *n*-pentane and *n*-nonane as limiting cases were conducted. The experimental results were compared with a high pressure evaporation model based on the Conduction Limit model and the Diffusion Limit model. The best agreement of measured and calculated values was obtained, when the theory of Abramzon and Sirignano (1987) was combined with the correlation of Ranz and Marshall (1952), and the specific heat capacity of the pure vapour was replaced by the specific heat capacity of the vapour/gas mixture.

Acknowledgement

The present study was supported by a grant from the SFB 167 (high intensity combustors) of the Deutsche Forschungsgemeinschaft.

References

[1] S. Wittig, W. Klausmann, B. Noll, J. Himmelsbach, Evaporation of fuel droplets in turbulent combustor flow, ASME-88-GT-107 (1988).
[2] Kneer, E. Benz, S. Wittig, Drop motion behind a prefilming airblast atomizer: comparison of phase doppler measurements with numerical predictions, Proceedings of the Fifth International Symposium on the Application of Laser Techniques to Fluid Mechanics, 1990.
[3] Hallmann, M. Scheurlen, S. Wittig, Computation of turbulent evaporating sprays: Eulerian versus Lagrangian approach, ASME-93-GT-333 (1993).
[4] Kurreck, M. Willman, S. Wittig, Prediction of the three-dimensional reacting two-phase flow within a jet-stabilized combustion, ASME-96-GT-468 (1996).
[5] K. Law, S. Prakash, W.A. Sirignano, Theory of convective, transient, multicomponent droplet vaporization, Proceedings of the 16th Symposium on Internal Combustion 1977, pp. 605–617.

[6] A. Sirignano, C.K. Law, Transient heating and liquid phase mass diffusion in droplet vaporization, Adv. Chemistry Series 166 (1978) 1–26.
[7] A. Manrique, G.L. Borman, Calculations of steady state droplet vaporization at high ambient pressures, International Journal of Heat and Mass Transfer 12 (1969) 1081–1095.
[8] C. Hsieh, J.S. Shuen, V. Yang, Droplet vaporization in high pressure environments I: near critical conditions, Combust. Sci. Tech. 76 (1991) 111–132.
[9] W. Curtis, P.V. Farrell, A numerical study of high-pressure droplet vaporization, Combust. Flame 90 (1992) 85–102.
[10] Jia, G. Gogos, High pressure droplet vaporization; effects of liquid-phase gas solubility, Int. J. Heat and Mass Transfer 36 (1993) 4419–4431.
[11] J. Stengele, H.-J. Bauer, S. Wittig. Numerical study of bicomponent droplet vaporization in a high pressure environment, ASME-96-GT-442 (1996).
[12] R. Wieber, Calculated temperature histories of vaporizing droplet to the critical point, AIAA Journal 1 (1963) 2764–2770.
[13] P. Delplanque, W.A. Sirignano, Numerical study of the transient vaporization of an oxygen droplet at sub- and super-critical conditions, Int. J. Heat and Mass Transfer 36 (1993) 303–314.
[14] L. Matlosz, S. Leipziger, T.P. Torda, Investigation of liquid drop evaporation in a high temperature and high pressure environment, Int. J. Heat and Mass Transfer 15 (1972) 831–852.
[15] Kadota, H. Hiroyasu, Evaporation of a single droplet at elevated pressures and temperatures, Bull. JSME 19 (1976) 1515–1521.
[16] Olthoff, Modellierung des Tropfenverdunstungsprozesses bei uberkirtischem Umgebungsdruck, DLR-Forschungsbericht, DLR-FB 93-54 (1994).
[17] Sato, M. Tsue, M. Niwa, M. Kono, Effects of natural convection on high pressure droplet combustion, Combust. Flame 82 (1990) 142–151.
[18] P. Hartfield, P.V. Farrell, Droplet vaporization in a high-pressure gas, Trans. ASME 115 (1993) 699–706.
[19] T. Shih, C. M. Megaridis, Suspended droplet evaporation modelling in a laminar convective environment, Combust. Flame 102 (1995) 256–270.
[20] Abramzon, W.A. Sirignano, Droplet vaporization model for spray combustion calculations, Int. J. Heat and Mass Transfer 32 (1989) 1605–1618.
[21] E. Ranz, W.R. Marshall, Evaporation from drops: parts I and II, Chem. Eng. Progress 48 (1952) 141–146, 173–180.
[22] K. Law, W.A. Sirignano, Unsteady droplet combustion with droplet heating—II: conduction limit, Combust. Flame 28 (1977) 175–186.
[23] B. Landis, A.F. Mills, Effect of diffusional resistance on the evaporation of binary droplets, Proceedings of the Fifth International Heat Transfer Conference, 1974.
[24] K. Aggarwal, Further results on evaporating bicomponent fuel sprays, Int. J. Heat and Mass Transfer 31 (1988) 2593–2597.
[25] Y. Tong, W.A. Sirignano, Multicomponent droplet vaporization in a high temperature gas, Combust. Flame 66 (1986) 221–235.
[26] D. Jin, G.L. Borman, A model for multicomponent droplet vaporization at high ambient pressures, SAE paper 850264, 1986.
[27] Stengele, M. Willmann, S. Wittig, Experimental and theoretical study of droplet vaporization in a high pressure environment, ASME-97-GT-151 (1997).
[28] Kneer, M. Schneider, B. Noll, S. Wittig, Effects of variable liquid properties on multicomponent droplet vaporization, Trans. ASME 115 (1993) 467–472.
[29] C. Reid, J.M. Prausnitz, B.E. Poling, The Properties of Gases and Liquids, McGraw-Hill Book Company, 1986.
[30] C. Reid, J.M. Prausnitz, T.K. Sherwood, The Properties of Gases and Liquids, McGraw-Hill Book Company, 1977.
[31] L.C. Lage, R.H. Rangel, Single droplet vaporization including thermal radiation absorption, J. Thermophys. Heat Transfer 7 (1993) 502–509.
[32] P. Delplanque, Liquid-oxygen droplet vaporization and combustion: analysis of transcritical behaviour and application to liquid-rocket combustion instability, Ph.D. thesis, University of California, Irvine, 1993.
[33] L. Hubbard, V.E. Denny, A.F. Mills, Droplet evaporation: effects of transient and variable properties, Int. J. Heat and Mass Transfer 18 (1975) 1003–1008.
[34] Renksizbulut, M.C. Yuen, Experimental study of droplet evaporation in a high temperature air stream, J. Heat Transfer 105 (1983) 384–388.
[35] C. Yuen, L.W. Chen, On drag of evaporating liquid droplets, Comb. Sci. and Technol. 14 (1976) 147–154.
[36] Renksizbulut, R.J. Haywood, Transient droplet evaporation with variable properties and internal circulation at intermediate Reynolds numbers, Int. J. Multiphase Flow 14 (1988) 189–202.
[37] W.J. Minkowycz, E.M. Sparrow, G.E. Schneider, R.H. Pletcher, Handbook of Numerical Heat Transfer, 1988, Wiley, New York, p. 104.